Tailoring amphotericin B as an ionic liquid: an upfront strategy to potentiate the biological activity of antifungal drugs†

Diego O. Hartmann, [a] Karina Shimizu, [b] Maika Rothkegel, [a] Marija Petkovic, [a] Ricardo Ferraz, [cd] Željko Petrovski, [e] Luís C. Branco, [e] José N. Canongia Lopes [b] and Cristina Silva Pereira *[a]

Aspergillus species are the primary cause of invasive aspergillosis, which afflicts hundreds of thousands of patients yearly, with high mortality rates. Amphotericin B is considered the gold standard in antifungal drug therapy, due to its broad-spectrum activity and rarely reported resistance. However, low solubility and permeability, as well as considerable toxicity, challenge its administration. Lipid formulations of amphotericin B have been used to promote its slow release and diminish toxicity, but these are expensive and adverse health effects of their prolonged use have been reported. In the past decades, great interest emerged on converting biologically active molecules into an ionic liquid form to overcome limitations such as low solubility or polymorphisms. In this study, we evaluated the biological activity of novel ionic liquid formulations where the cholinium, cetylpyridinium or trihexyltetradecylphosphonium cations were combined with an anionic form of amphotericin B. We observed that two formulations increased the antifungal activity of the drug, while maintaining its mode of action. Molecular dynamics simulations showed that higher biological activity was due to increased interaction of the ionic liquid with the fungal membrane ergosterol compared with amphotericin B alone. Increased cytotoxicity could also be observed, probably due to greater interaction of the cation with cholesterol, the main sterol in animal cells. Importantly, one formulation also displayed antibacterial activity (dual functionality), likely preserved from the cation. Collectively, the data set ground for the guided development of ionic liquid formulations that could improve the administration, efficacy and safety of antifungal drugs or even the exploitation of their dual functionality.

[a] Instituto de Tecnologia Química e Biológica António Xavier, Universidade Nova de Lisboa (ITQB NOVA), Av. da República, Oeiras, 2780-157, Portugal. E-mail: spereira@itqb.unl.pt

[b] Centro de Química Estrutural, Instituto Superior Técnico, Universidade de Lisboa, Av. Rovisco Pais, 1049-001 Lisboa, Portugal

[c] Ciências Químicas e das Biomoléculas (CQB) e Centro de Investigação em Saúde e Ambiente (CISA), Escola Superior de Saúde do Instituto Politécnico do Porto, 4400-330 Porto, Portugal

[d] LAQV-REQUIMTE, Departamento de Química e Bioquímica, Faculdade de Ciências, Universidade do Porto, Rua do Campo Alegre 687, 4169-007 Porto, Portugal

[e] LAQV-REQUIMTE, Departamento de Química, Faculdade de Ciências e Tecnologia da Universidade Nova de Lisboa, 2829-516 Caparica, Portugal

† Electronic supplementary information (ESI) available. See DOI: 10.1039/d1ra00234a

Introduction

Invasive fungal infections present a severe threat worldwide. The genus *Aspergillus* includes some of the most common airborne fungi and opportunistic pathogens, allergen and mycotoxin producers.[1] *Aspergillus fumigatus* is the primary cause of invasive aspergillosis, which affects over two thousand hundred immunocompromised patients per year, with a mortality rate of 50% even if diagnosed and treated at early stages.[1,2] It has been demonstrated that *A. fumigatus* forms biofilms *in vivo*, *i.e.* a growth mode that implies tightly associated hyphae embedded in an extracellular polymeric matrix.[3] These biofilm cultures appear to be significantly more resistant to antifungal agents than free-living cultures, probably due to reduced diffusion rates of antifungal agents through the extracellular matrix, as well as an increased activity of efflux pumps and transporter proteins.[3,4]

The arsenal of antifungal drugs currently in clinical use is rather limited and relays mainly on targeting ergosterol – the main fungal sterol – or its biosynthetic pathway (polyenes and azoles), fungal cell wall (echinocandins) or nucleic acids synthesis (pyrimidine analogs).[5] Resistance to azoles (which target a 14α-demethylase in ergosterol biosynthesis)[6] and, more recently, to echinocandins (due to mutations in cell wall biosynthetic genes)[7] have been already reported and it is assumed to be a consequence of their excessive use. The macrolide polyene amphotericin B (AmB), on the other hand, remains a gold standard in antifungal drug therapy, due to its

relatively broad spectrum of action and uncommon emergence of resistance during treatment.[8] AmB preferentially binds to ergosterol, the primary sterol in the fungal cell membrane. As a consequence, there is a disruption of the osmotic integrity of the membrane, with leakage of ions and other cellular materials and, consequently, death.[9] The most commonly accepted mode of action assumes that AmB forms ion channel aggregates that are inserted in the lipid bilayer, causing its permeabilization.[10] A sterol sponge model proposed that AmB exists in the form of large extramembranous aggregates that extract ergosterol from the lipid bilayers instead.[11] Transcriptomic and proteomic analysis of *A. fumigatus* after exposure to AmB further revealed its molecular targets, mainly in the ergosterol biosynthetic pathway, cell wall maintenance, cell stress and transport proteins.[12] Oxidative stress has been implicated as critical for cell death and likely has an important role in AmB mechanism of action; however, direct proof is still lacking.[13]

The amphipathic nature of AmB, along with its low solubility and permeability, has always posed as a great disadvantage in its administration. AmB itself is insoluble in saline at a physiological pH and therefore it is normally prescribed in a combination with the detergent sodium deoxycholate. The major drawback in the use of amphotericin B deoxycholate is its narrow therapeutic index, namely high toxicity manifested as acute infusion-related reactions and dose-related nephrotoxicity.[14] Since its first clinical use in 1959, three lipid formulations of AmB were commercialized (*i.e.* colloidal dispersion, lipid complex and liposomal AmB), as to promote slow release and diminish toxic side-effects.[15] These formulations, however, are considerably expensive, and some reports indicate adverse health effects of their prolonged use.[16] In the past years, new promising solutions to overcome AmB limited solubility and high toxicity have emerged, such as poly(D,L-lactide-*co*-glycolide) nanoparticles with AmB.[17] Noteworthy is a study in which several ionic liquids were designed and used as excipients for AmB, achieving some improvement in drug solubility.[18]

Ionic liquids are a class of tuneable organic salts that have been largely studied as catalysts or solvents for industrial and biotechnological applications.[19,20] In the past decade, we have witnessed the conversion of biologically active molecules to an ionic liquid form to overcome limitations such as low solubility or polymorphisms,[21] *e.g.* ranitidine docusate,[22] cholinium betulinate[23] or cholinium niflumate.[24] The strategy of transforming commonly used antibiotics,[25,26] herbicides[27] or fungicides[28] to an ionic liquid form was also undertaken. As an example, the antibiotic ampicillin was combined with several cations, such as cetylpyridinium ($[C_{16}py]^+$), trihexyltetradecylphosphonium ($[P_{6,6,6,14}]^+$) or cholinium ($[chol]^+$).[25] Some of the resulting ampicillin ionic liquids were observed to be significantly more effective against a variety of clinically relevant bacteria, especially resistant strains.

In this study, we evaluated the biological activity of new ionic liquid formulations where the $[chol]^+$, $[C_{16}py]^+$ or $[P_{6,6,6,14}]^+$ cations were coupled with an anionic form of AmB ($[AmB]^-$) (Fig. 1). The resulting cholinium amphotericin B ([chol][AmB]), cetylpyridinium amphotericin B ($[C_{16}py][AmB]$) and trihexyltetradecylphosphonium amphotericin B ($[P_{6,6,6,14}][AmB]$) were subjected to various
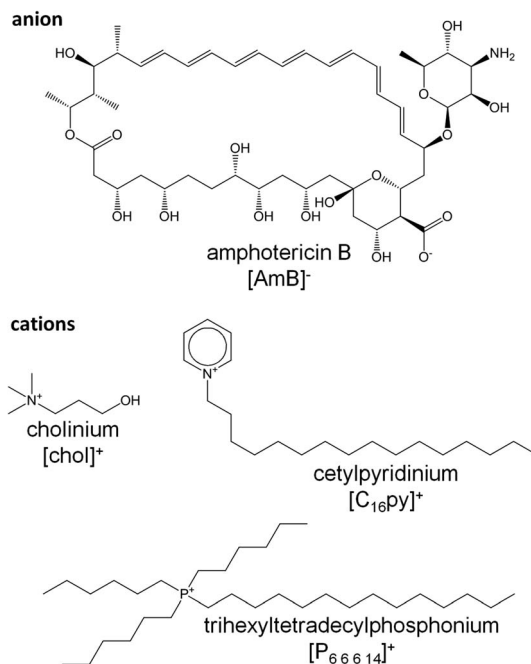

Fig. 1 Anion and cations structures present in the amphotericin B-ionic liquid formulations used in this study: cholinium amphotericin B ([chol][AmB]), cetylpyridinium amphotericin B ($[C_{16}py][AmB]$) and trihexyltetradecylphosphonium amphotericin B ($[P_{6,6,6,14}][AmB]$).

susceptibility assays to determine if they displayed increased antifungal activity against *Aspergillus* biofilm cultures, when compared with the parent antifungal drug, *i.e.* AmB. We performed gene expression analysis to confirm if the responsive genes and mode of action of AmB were kept the same. Molecular dynamics simulations studies were done to further investigate the mechanisms behind different susceptibility patterns observed between AmB and the ionic liquid formulations.

Experimental

Chemicals

Commercially available reagents were purchased from Sigma-Aldrich, BDH Laboratory Reagents, Frilabo and Solchemar (unless stated otherwise). The solvents were from Valente & Ribeiro and distilled before used. The basic anion-exchange resin Amberlite IRA-400-OH (ion-exchange capacity 1.4 eq. per mL) was purchased from SUPELCO. The synthetized ionic liquids were characterized by IR spectroscopy (PerkinElmer 683 spectrometer) and by ^1H and ^{13}C NMR spectroscopy (Bruker AMX400 spectrometer) and their purity was confirmed by Matrix Assisted Laser Desorption Ionization-Time of Flight (MALDI-TOF). 5 mM stock solutions in DMSO were prepared and kept at -20 °C. 100 mM stocks were also made for $[C_{16}py]Cl$ and $[P_{6,6,6,14}]Cl$ and a 2.5 M stock was made for [chol]Cl (in water).

Synthesis of amphotericin B-based ionic liquids

For the synthesis of cholinium amphotericin B ([chol][AmB]), cetylpyridinium amphotericin B ($[C_{16}py][AmB]$) and

trihexyltetradecylphosphonium amphotericin B ($[P_{6,6,6,14}]$[AmB]), (2-hydroxyethyl)-trimethylammonium chloride, cetyl-pyridinium chloride or trihexyl(tetradecyl)phosphonium chloride, respectively, was dissolved in methanol and passed through an ion-exchange Amberlite IRA-400(OH) (5 eq., flux rate 0.133 mL min^{-1} = 8 BVh^{-1}). Each hydroxide solution formed was slowly added to amphotericin B dissolved in 1.0 M dried triethylamine methanolic solution. Each mixture was stirred at room temperature for 1 hour. After solvent evaporation the residue was dried *in vacuum* for 24 hours to provide the desired products. Detailed data on the synthesis and characterization of each AmB ionic liquid are described in ESI.†

Fungal susceptibility assays

The fungal strains *Aspergillus fumigatus* Af293 and *Aspergillus terreus* NIH2624 were purchased from the Fungal Genetics Stock Centre (Table S1†). Cultures were grown on Sabouraud dextrose agar at 37 °C and conidial suspensions were prepared and stored at −20 °C in 20% glycerol until use. The method used in the susceptibility assays was a modified version of that proposed by Mowat *et al.*[4] The cultivation medium was RPMI 1640 (Sigma-Aldrich, R0883), supplemented with glutamine (0.3 g L^{-1}), glucose (10 g L^{-1}) and 0.165 M MOPS, and buffered to pH 7.0. All procedures were carried out in an ESCO Class II Biosafety Cabinet. *Aspergillus fumigatus* and *A. terreus* biofilms were formed on sterile, polystyrene, flat-bottomed, 96-well microtiter plates (Corning). 200 μL of conidial suspension (10^5 conidia per mL) in MOPS-buffered RPMI 1640 was added to each well and incubated statically for 24 hours at 37 °C. A minimum of five replicates was performed for each experimental parameter, plus suitable controls (DMSO control, negative control and blank wells). After 24 hours, the biofilms were formed; the medium was aspirated and replaced by serial double dilutions of the compounds. The selected concentrations varied for each compound. The range was from 0.03125 to 32 μM for AmB-based compounds, 0.098 to 200 μM for [C_{16}py]Cl and [$P_{6,6,6,14}$]Cl and 1 μM to 1 M for [chol]Cl. The challenged biofilm cultures were incubated for additional 24 hours at 37 °C. Metabolic activity reduction was assessed using a standard MTT assay, in comparison to untreated culture. Briefly, a solution of 3-(4,5-dimethylthiazol-2-yl)-2,5-diphenyl tetrazolium bromide (MTT) was added to each well at a final concentration of 0.438 mg mL^{-1}, and then incubated for further 4 hours. Afterwards the supernatant medium was removed and replaced by 0.04 M HCl in isopropanol to dissolve the formed formazan crystals. MTT reduction was monitored with a micro-plate reader scoring absorbance at 570 nm. The same method was used to evaluate the interaction of [C_{16}py]Cl and AmB in a checkerboard assay.[29] Each experiment was repeated on at least three separate occasions. Statistical analysis was performed using Graph Prism v7.0. Independent experiments were compared using one-way ANOVA analysis of variance and Bonferroni's multiple comparison test and no significant differences were observed. The half-minimal inhibitory concentrations (IC$_{50}$, *i.e.* the concentration of the test substance that lowers MTT reduction by 50% when compared to the untreated control) were calculated from dose–response curves. The curves of each treatment were compared using paired Student's *t*-test with 95% confidence interval.

Gene expression analysis

A suspension of 10^5 *A. fumigatus* conidia per mL of medium was incubated in 50 mL of MOPS-buffered RPMI 1640 medium (as described above). Triplicate biofilm cultures were cultivated in 75 cm^2 surface-treated cell culture flasks. After 24 hours of growth, AmB, [chol][AmB], [C_{16}py][AmB] or [$P_{6,6,6,14}$][AmB] were added to the culture media to obtain a final concentration corresponding to the IC$_{50}$ of each compound and incubated for 4 or 24 hours. A negative control without the addition of any compound was also included. Afterwards, mycelia were recovered by filtration (0.45 μm membrane filters, Millipore) and immediately frozen in liquid nitrogen. Approximately 100 mg of frozen mycelia were ground with poly(vinylpolypyrrolidone) (0.4 mg per mg of mycelia) using a TissueLyser LT (QIAGEN). The final powder was used in the extraction and purification of total RNA using the RNeasy Plant Mini Kit (QIAGEN), according to the manufacturer's protocol. Genomic DNA digestion was done with the RNase-Free DNase Set (QIAGEN). Quality, integrity and quantity of the total RNA were analyzed using a Nano-Drop 1000 spectrophotometer (Thermo Scientific) and by running 2 mg of RNA into 1% agarose gels in TAE buffer. The complementary DNA (cDNA) was synthesized from 500 ng of the total RNA using an iScript cDNA Synthesis Kit (Bio-Rad) in a T100 Thermal Cycler (Bio-Rad). The reaction protocol consisted of 5 min at 25 °C, 30 min at 42 °C and 5 min at 85 °C.

For the gene expression analysis by quantitative real-time PCR (qRT-PCR), oligonucleotide pairs for nine specific AmB-responsive *A. fumigatus* genes (Table S2†) were designed using the Gene-Fisher2 web tool (http://bibiserv.techfak.uni-bielefeld.de/genefisher2), and produced by STAB VIDA. The qRT-PCR analysis was performed in a CFX96 Thermal Cycler (Bio-Rad), using a SsoFast EvaGreen Supermix (Bio-Rad), 250 nM of each oligonucleotide and the cDNA template equivalent to 10 ng of the total RNA, at a final volume of 10 μL per well, in three technical replicates. The PCR conditions were: enzyme activation at 95 °C for 30 s; 40 cycles of denaturation at 95 °C for 10 s and annealing/extension at 59 °C for 10 s; and a melting curve obtained from 65 °C to 95 °C, consisting of 0.5 °C increments for 5 s. Data analyses were performed using the CFX Manager software (Bio-Rad). The expression of each gene was normalized by the expression of the glyceraldehyde-3-phosphate dehydrogenase gene (*gpdA*, internal control). The final expression values were obtained as a relative expression comparatively to the negative control, for each target gene. Three biological replicates were performed. Statistical analysis was performed in the GraphPad Prism v7.0 software. Treatments with ionic liquids formulations were compared with AmB for each time point (4 and 24 hours) by multiple Student's *t*-test. Differences with a *P* value below 0.05 were considered statistically significant.

Cytotoxicity assay

Cell line mIMCD-3 (ATCC® CRL-2123™) from mouse (*Mus musculus*) inner medulla collecting duct was kindly provided by

Dr Duarte C. Barral (Chronic Diseases Research Center, NOVA Medical School, Lisbon, Portugal). Cells with a passage number between six and 21 were used. Cells were cultured in Dulbecco's modified eagle medium: nutrient mixture F-12 supplemented with fetal calf serum (10% v/v) and 1% Pen–Strep preparation (all from Life Technologies). 96-well micro-plates were used for MTT assays, using the two-fold dilutions of the tested compounds. Equal volumes of cell suspension and test solution in culture media were added to each well, to obtain final volume of 150 μL with 7.5×10^4 cells. The plates were incubated for 68 hours at 37 °C in a 5% CO_2 atmosphere. A solution of MTT was then added to each well to reach a final concentration of 3.6 mg mL^{-1}, and then incubated as before for further 4 hours. Afterwards, the supernatant media was removed and substituted by acidified (0.02 M HCl) 10% v/v SDS solution, followed by overnight incubation in the dark at room temperature. At the end of the experiment, MTT reduction was monitored with a micro-plate reader scoring absorbance at 570 nm.

Molecular dynamics simulations

The [C$_{16}$py][AmB] formulation was parameterized using the CL&P atomistic force field,[30] an extension of the AMBER and OPLS force fields,[31] specially designed to study ionic liquids and their homologous series. Water, ergosterol, cholesterol, AmB and [AmB]$^-$ anion were modeled using the SPC model[32] and the OPLS force field, respectively. Molecular dynamics simulations were carried out using the DL_POLY 2.20 package[33] and Gromacs package.[34–38] The runs in DL_POLY started from low-density configurations built with the PACKMOL package[39] and were performed using 2 fs time steps and 2 nm cut-off distances. All simulations were subjected to equilibration runs under isobaric isothermal ensemble conditions (p = 0.1 MPa and T = 300 K with Nosé–Hoover thermostats and barostats with relaxation time constants of 1 and 4 ps, respectively) for 200 ps. Therefore, Gromacs simulations were performed using 2 fs time steps and 2 nm cut-off distances, with Ewald summation corrections performed beyond the cut-offs. The isothermal–isobaric ensemble conditions used during equilibration were p = 0.1 MPa and T = 300 K with V-rescale thermostats and Berendsen barostats with relaxation time constants of 1 and 4 ps, respectively. Nine consecutive runs were carried out to conduct an annealing process. The temperature range was from 300 K to 500 K. After 10 ns, the density of each system reached constant and consistent values, indicating that equilibrium had been attained and possible ergodicity problems were overcome. Finally, 10 ns production stage was performed using 1 fs time step; the isothermal–isobaric ensemble conditions used during equilibration were p = 0.1 MPa and T = 300 K with Nosé–Hoover thermostats and Parrinello–Rahman barostats with relaxation time constants of 1 and 4 ps, respectively. The aqueous solutions containing the ergosterol or cholesterol and AmB or [C$_{16}$py][AmB] were modeled using one sterol molecule and two AmB or [C$_{16}$py][AmB] molecules mixed with 4000 water molecules. Three different complexes were produced for each mixture. All simulations were performed as described above. The most stable complexes were chosen (Table

S3†). Low density initial configurations were randomly built using the Packmol package, placing ten complexes mixed with 10 000 water molecules, and then new simulations were performed.

The aggregation analyses of ergosterol, cholesterol, AmB and [C$_{16}$py][AmB] mixtures with water focused on two types of issues: (i) the evaluation of the connectivity among the ergosterol or cholesterol molecules and an estimation of their aggregate sizes; and (ii) the calculation of the connectivity between the AmB or [C$_{16}$py][AmB] and the ergosterol or cholesterol molecules. All these types of connectivity analyses were based on previously described algorithms[40] that generate neighbor lists for selected interaction centers, in a three-stage sequential process. First, the different types of interaction centers were defined. In type (i) analyses the selected interaction centers were all non-hydrogen atoms in the ergosterol or cholesterol molecules. Type (ii) analyses were conducted by selecting all carbon atoms of the alkyl chain of the cation or carbon atoms of the unsaturated part of the AmB or [C$_{16}$py][AmB], and all non-hydrogen atoms in the ergosterol or cholesterol molecules. Second, a connectivity threshold for each case was established by considering the corresponding $g_{ij}(r)$ data between the selected interaction centers.[40] In cases (i) and (ii) the threshold was set to 0.5 nm, corresponding to average intermolecular contact distances between non-hydrogen atoms evaluated from the corresponding $g(r)$ functions. Third, the use of the threshold criteria allowed the computation of closest-neighbor lists for each interaction center for all recorded configurations in the molecular dynamics trajectories, thus ascertaining the connectivity between the selected species. When the interaction centers belonged to species of the same type, i.e. sterol–sterol in case (i), the corresponding aggregates corresponded to clusters containing a single type of molecule. In the case of interaction centers belonging to different species, i.e. sterol–AmB or sterol–[C$_{16}$py][AmB] in case (ii), the analyses yielded aggregates with a built-in between species.

High-performance liquid chromatography (HPLC) analyses

To mimic the conditions from the molecular dynamics simulations, ergosterol was incubated in water with either AmB, [C$_{16}$py][AmB] or [C$_{16}$py]Cl. 20 μM of ergosterol was mixed with 20, 30, 40, 50 or 60 μM of each compound (from the DMSO stock solution) in ultrapure water, at a final volume of 1 mL, at room temperature, for one hour. Ergosterol with equal concentrations of DMSO as each condition was used as control. After incubation, the mixtures were centrifuged at 25 000g for 10 min, the supernatant was recovered and ergosterol content was analyzed on a Waters HPLC System with a 2707 Autosampler, a 1525 binary HPLC pump with a column oven, and a 2998 Photodiode Array Detector. A Symmetry® C18 reverse phase column (250 × 4.6 mm), packed with end capped particles (5 μm, pore size 100 Å) was used at 30 °C. Data were acquired using Empower 2 software, 2006 (Waters Corporation). Sample injections of 50 μL were made using a 100 μL loop operated in partial loop mode. The mobile phase, at a flow rate of 1.2 mL min^{-1}, consisted of 90% methanol and 10% acetonitrile. Each sample was run for

17 min. Ergosterol was detected at 282 nm and eluted at 13 min. Ergosterol was quantified by peak area according to a calibration curve. Three replicates of each condition were performed. Ergosterol content in the supernatant of mixtures of AmB, $[C_{16}py][AmB]$ or $[C_{16}py]Cl$ was taken relative to the control.

Antibacterial activity assays

The ionic liquid formulation $[C_{16}py][AmB]$ and its parental compounds AmB and $[C_{16}py]Cl$ were assessed for their antimicrobial activity against *Staphylococcus aureus* NCTC8325 and *Escherichia coli* TOP 10 strains. The bacteria were grown to approximately 1 to 2×10^8 CFU mL^{-1} in Mueller Hinton Broth (MHB, Panreac). Two-fold serial dilutions of each compound were performed to obtain final concentrations between 0.195 and 100 μM, in 96-well plates, in triplicates. Abiotic (medium alone) and biotic controls (without addition of any compound) were included for each test. Plates were incubated statically at 37 °C for 24 hours and absorbance (600 nm) was measured at the end of incubation using a Tecan Infinite 200 Microplate spectrophotometer (Männedorf, Switzerland). At least three biological replicates were performed. Statistical analysis and determination of IC$_{50}$ values were done as described for the fungal susceptibility assays.

Results and discussion

In this study, we investigated the biological activity of new ionic liquid formulations of AmB, which were designed as an alternative to overcome the low solubility of this antifungal drug. The anionic form of AmB was combined with three different cations, namely $[chol]^+$, $[C_{16}py]^+$ or $[P_{6,6,6,14}]^+$ (Fig. 1). $[chol]^+$ is a well-known nutraceutical (in the form of cholinium chloride),[41] and has been proposed in many ionic liquid formulations as a non-toxic and biodegradable cation.[42] $[C_{16}py]^+$ has been widely used, mainly in its chloride form, as an antimicrobial agent in oral hygiene products[43] and in some ionic liquids formulations combined with active pharmaceutical ingredients, *e.g.* aspirin.[44] Despite the considerably high toxicity of $[P_{6,6,6,14}]^+$,[45] this cation has already been successfully used in the development of antibiotic ionic liquid formulations, increasing the biocidal activity of ampicillin,[25] amoxicillin and penicillin G[26] against resistant bacterial strains.

Antifungal activity against *Aspergillus fumigatus*

We evaluated the susceptibility of *A. fumigatus* to the synthesized formulations $[chol][AmB]$, $[C_{16}py][AmB]$ and $[P_{6,6,6,14}][AmB]$, comparatively to the effect of their parental compounds. While the antifungal drug AmB presented an IC$_{50}$ of 0.70 μM, the parental compounds $[chol]Cl$, $[C_{16}py]Cl$ and $[P_{6,6,6,14}]Cl$ presented much lower activity against *A. fumigatus*, with IC$_{50}$ of 880 mM (approximate value), 12.78 μM and 28.4 μM, respectively (Fig. 2). An initial comparison of the dose–response curves showed that both ionic liquid formulations $[chol][AmB]$ and $[C_{16}py][AmB]$ appear to be more effective than AmB (Fig. 2). However, the statistical analysis revealed that only $[C_{16}py][AmB]$ presents a dose–response curve significantly different from AmB (P value: 0.0008),
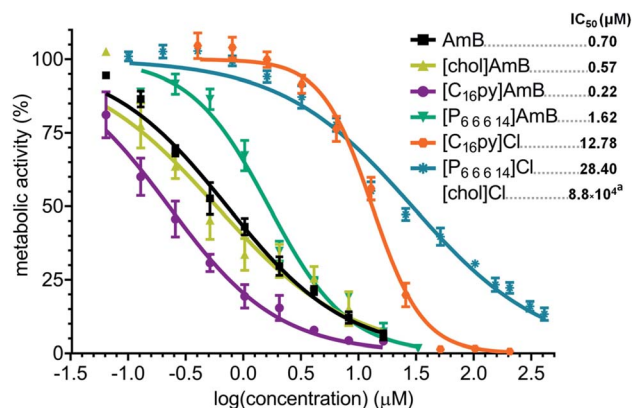

Fig. 2 Dose–response curve and calculated IC$_{50}$ values (in μM, upper right corner) of amphotericin B (AmB, black squares), cholinium amphotericin B ($[chol][AmB]$, yellow triangles), cetylpyridinium amphotericin B ($[C_{16}py][AmB]$, purple circles), trihexyltetradecylphosphonium amphotericin B ($[P_{6,6,6,14}][AmB]$, green inverted triangles), cetylpyridinium chloride ($[C_{16}py]Cl$, orange hexagons), trihexyltetradecylphosphonium chloride ($[P_{6,6,6,14}][AmB]$, blue asterisks) and cholinium chloride against *Aspergillus fumigatus*. The y axis represents the percentage of metabolic activity (determined by standard MTT assay) comparatively to the growth without any treatment. The x axis represents the log of the concentration of each tested compound. [a]For cholinium chloride, the curve was omitted since most tested concentrations displayed no inhibition of activity and the IC$_{50}$ value is an approximate prediction based on the obtained data.

while the differences between the curves of $[chol][AmB]$ and the parental compound are not statistically significant (P value: 0.4674). Despite that, both ionic liquid formulations showed lower calculated IC$_{50}$ values than AmB (determined in this study as 0.70 μM). $[chol][AmB]$ and $[C_{16}py][AmB]$ displayed IC$_{50}$ values of 0.57 and 0.22 μM, respectively, representing an increase in the antifungal activity of *ca.* 1.2 and 3.2-fold. Interestingly, despite showing a significantly different dose–response curve compared to AmB (P value: 0.0292), the $[P_{6,6,6,14}][AmB]$ formulation had an opposite effect and decreased the activity of AmB, with a calculated IC$_{50}$ of 1.62 μM (Fig. 2).

Expression analyses of AmB-responsive genes

The susceptibility data showed that the ionic liquid formulations of AmB were able to alter the dose necessary to affect the growth of *A. fumigatus*, but whether the mode of action of the antifungal drug were kept the same was still unclear. To address this question, we analyzed the expression of *A. fumigatus* genes known to be responsive to AmB. Based on transcriptomic and proteomic analysis of *A. fumigatus* after exposure to AmB,[12] we selected a set of nine genes that belong to main functional groups with increased expression upon AmB exposure: ergosterol biosynthesis (sterol 24-C-methyltransferase – *erg6*; 14-α-demethylase – *erg11B*; and hydroxymethyl glutaryl-coenzyme A synthase – *erg13*), cell stress (manganese superoxide dismutase – *sod3*; and putative glutathione *S*-transferase, "GST"), cell wall proteins (conidial cell wall hydrophobin – *rodB*) and transporter proteins (multidrug resistance protein4 – *mdr3*, plasma membrane H$^+$ ATPase – *pma1*; and putative GTPase-activating

protein, "GTPase"). These genes have been previously reported to be up-regulated after 24 hours of exposure to AmB.[12]

In our study, we analyzed the expression of these nine genes after 4 or 24 hours of exposure to AmB, [chol][AmB], [C$_{16}$py][AmB] and [P$_{6,6,6,14}$][AmB], relatively to a negative control. We observed that, after 4 hours of exposure to AmB, all the tested genes underwent a great down-regulation in their expression (Fig. 3 and Table S4†). With the exception of *mdr3* (that had a 5.5-fold increase), we did not observe a considerable increase in the expression of the genes after 24 hours of exposure to AmB relative to the negative control (Fig. 3 and Table S4†). However, we observe that the genes underwent an up-regulation in their expression compared to 4 hours of exposure. These results are consistent with other studies that reported major decreases in the expression of responsive genes within the first hours of AmB exposure, followed by their increase afterwards.[12,46]

After 4 hours of exposure to [chol][AmB] or [C$_{16}$py][AmB], the majority of the responsive genes (five for [chol][AmB] and six for [C$_{16}$py][AmB], out of nine tested genes) displayed expression profiles with no significant differences from AmB (Fig. 3 and Table S4†). This similarity is even more evident after 24 hours of exposure to the ionic liquid formulations. Eight out of nine of the tested genes, either for [chol][AmB] or [C$_{16}$py][AmB], had expression levels with no significant differences from the AmB treatment (Fig. 3 and Table S4†). These results indicate that redesigning AmB as [chol][AmB] or [C$_{16}$py][AmB] did not alter the molecular response of the fungus, suggesting the preservation of its mechanism of action in these ionic liquid formulations. This was not observed for the [P$_{6,6,6,14}$][AmB], since all or nearly all genes had significantly different expression levels compared to AmB, either for 4 or 24 hours (Fig. 3 and Table S4†). Quaternary phosphonium-based ionic liquids, *e.g.* alkyltributylphosphonium chlorides, have been previously described to inhibit the growth and completely kill *A. nidulans* at concentrations above 10 μM, mainly by inducing damage to the fungal cell wall and plasma membrane.[47,48] In this study, although [P$_{6,6,6,14}$]Cl displayed inhibition values comparable to those reported in the literature for similar compounds, its
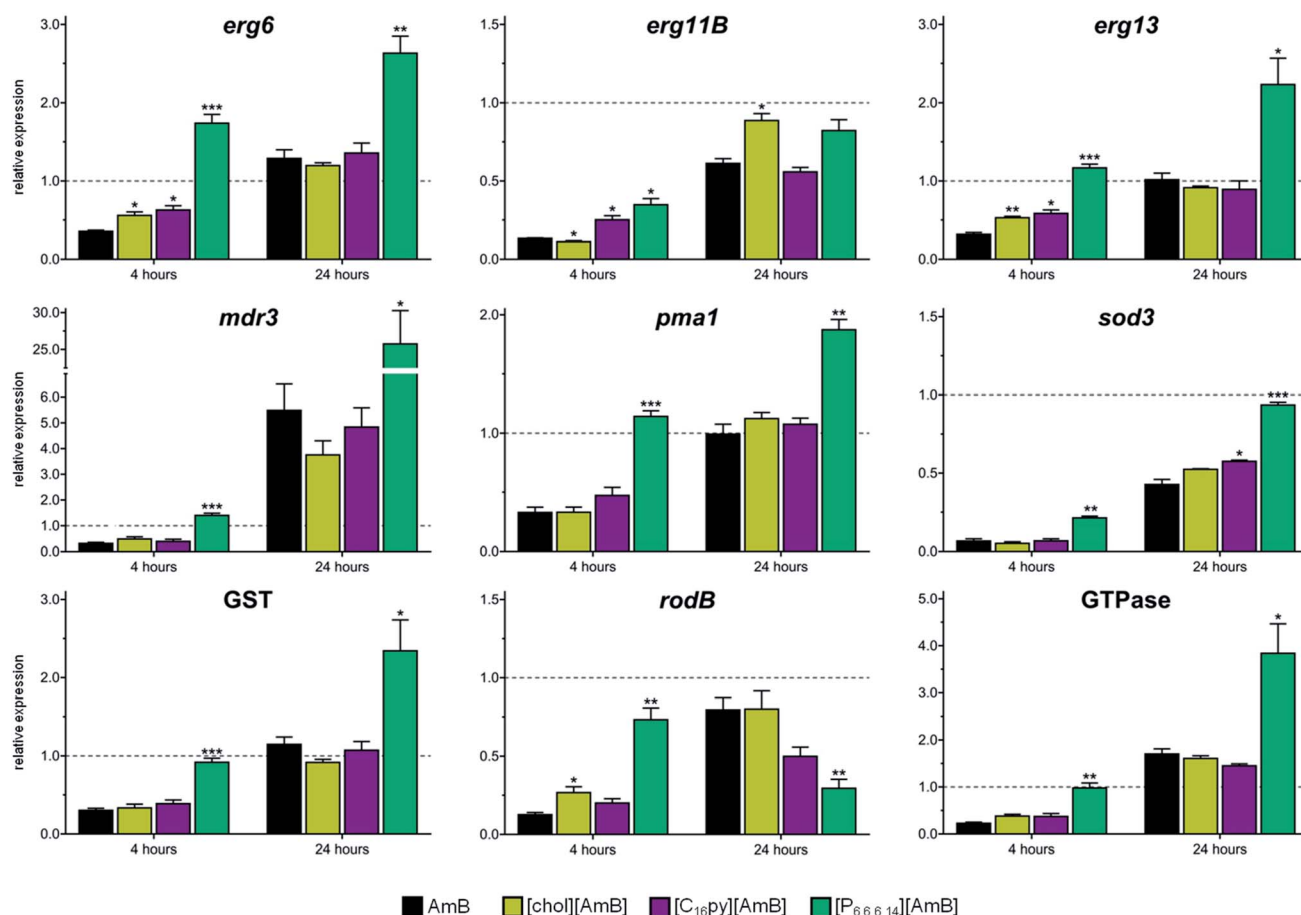

Fig. 3 Gene expression analysis of nine amphotericin B-responsive genes in *Aspergillus fumigatus* (*erg6*, *erg11B*, *erg13*, *mdr3*, *pma1*, *sod3*, putative glutathione *S*-transferase gene (GST, Afu3g07930), *rodB* and putative GTPase gene (Afu6g12340)) after 4 or 24 hour exposure to amphotericin B (AmB, black bars), cholinium amphotericin B ([chol][AmB], yellow bars), cetylpyridinium amphotericin B ([C$_{16}$py][AmB], purple bars) or trihexyltetradecylphosphonium amphotericin B ([P$_{6,6,6,14}$][AmB], green bars). Glyceraldehyde 3-phosphate dehydrogenase gene (*gpdA*) was used as internal control. Values represent the fold-change relative to the negative (untreated) control followed by their standard deviation. Three biological replicates were performed. The asterisks mark statistically significant differences in the expression of [chol][AmB], [C$_{16}$py][AmB] or [P$_{6,6,6,14}$][AmB] when compared to AmB for each exposure time (* = $p < 0.05$; ** = $p < 0.01$, *** = $p < 0.001$).

combination with AmB in an ionic liquid form decreased the activity and altered the fungal response to the parental antifungal drug. $[P_{6,6,6,14}]Cl$ has a strong hydrophobic nature;[49] it is possible that its combination with AmB (also highly hydrophobic) greatly decreases the bioavailability of the antifungal drug, therefore its activity. Having the lower activity of $[P_{6,6,6,14}][AmB]$ in consideration, the following studies focused on [chol][AmB] and $[C_{16}py][AmB]$ formulations.

Antifungal activity against intrinsically resistant *Aspergillus terreus*

Considering their higher antifungal activity towards *A. fumigatus* and preserved mechanism of action, we asked if other fungal species would also be more susceptible to [chol][AmB] or $[C_{16}py][AmB]$, compared to AmB. We selected *A. terreus*, which is also an important causative agent of invasive fungal infections and that, more importantly, presents an intrinsic resistance to AmB.[13,50] In our study, AmB had a calculated IC_{50} of 2.60 μM against *A. terreus* (Fig. 4), almost four times higher than that determined for *A. fumigatus* (Fig. 2). The parental compounds [chol]Cl and $[C_{16}py]Cl$ displayed low antifungal activity, with IC_{50} values of 1.08 M (approximate value) and 11.85 μM, respectively (Fig. 4). When testing [chol][AmB] and $[C_{16}py][AmB]$ against *A. terreus*, we observed that both formulations showed significantly different dose–response curves when compared to AmB (*P* values: 0.0133 and 0.0009, respectively) (Fig. 4). [chol][AmB] had an IC_{50} of 2.11 μM, while $[C_{16}py][AmB]$ displayed a calculated IC_{50} of 0.82 μM, which represent *ca.* 1.2 and 3.2-fold increase in AmB activity, respectively, the same levels observed for *A. fumigatus* (Fig. 2).

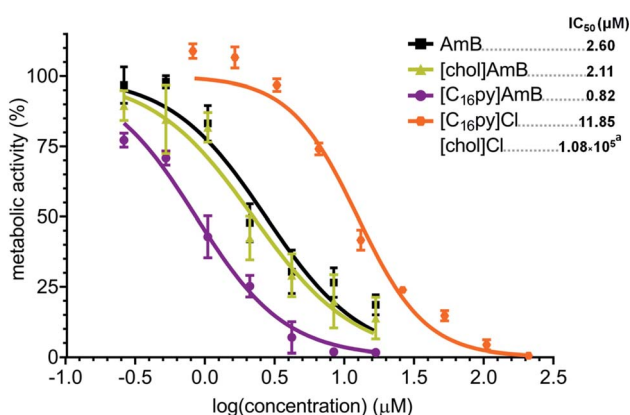### Influence of an ionic liquid form

As previously reported for ionic liquids based on ampicillin,[25] amoxicillin and penicillin G,[26] combination of AmB with the $[C_{16}py]^+$ cation also resulted in the most active formulation. Our data showed that $[C_{16}py][AmB]$ displayed significant differences in dose–response curves and the highest antifungal activity for both fungi, while likely maintaining the mode of action of AmB. For these reasons, this ionic liquid was selected to further investigate the mechanisms behind this increased biological activity. Initially, we aimed at understanding if an ionic liquid formulation, rather than a simple synergy between the parental compounds, was essential for the increased activity of $[C_{16}py][AmB]$. We performed a checkerboard assay,[29] where we tested the susceptibility of *A. fumigatus* to combinations of different concentrations of cetylpyridinium chloride ($[C_{16}py]Cl$) and AmB. The equimolar combination of both compounds produced a dose–response curve that was significantly different from those of $[C_{16}py]Cl$ (*P* value: 0.0105) and AmB (*P* value: 0.0473) alone, and also from the curve obtained for $[C_{16}py][AmB]$ (*P* value: 0.0133) (Fig. 5). It appears that addition of $[C_{16}py]Cl$ to a neutral AmB actually decreases the activity of the latter, as seen by the calculated IC_{50} of 1.58 μM. This value is *ca.* eight times lower than the IC_{50} of $[C_{16}py]Cl$ (12.58 μm), but more than double of that for AmB alone (0.70 μM) and more than seven times higher than the IC_{50} of $[C_{16}py][AmB]$ (0.22 μm) (Fig. 5). An ionic liquid formulation, that combines a cation such as $[C_{16}py]^+$ and the anionic form of AmB ($[AmB]^-$) anion, seems to be necessary for increased antifungal activity. Even though further evidence is be necessary, the enhanced antifungal activity observed in our study could be a consequence of $[C_{16}py]^+$ and $[AmB]^-$ acting as pair, instead of dissociated ions. This is in line with the idea of the existence of ion-pairing in ionic liquids,[51] which is already believed to be behind some of the physical properties of these class of compounds.[52]
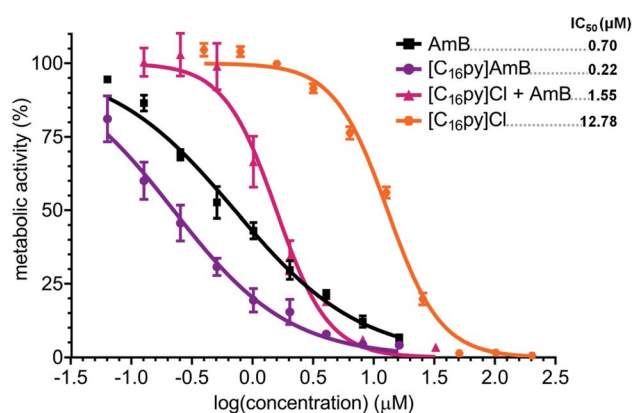

Fig. 4 Dose–response curve and calculated IC_{50} values (in μM, upper right corner) of amphotericin B (AmB, black squares), cholinium amphotericin B ([chol][AmB], yellow triangles), cetylpyridinium amphotericin B ($[C_{16}py][AmB]$, purple circles), cetylpyridinium chloride ($[C_{16}py]Cl$, orange hexagons) and cholinium chloride against *Aspergillus terreus*. The *y* axis represents the percentage of metabolic activity (determined by standard MTT assay) comparatively to the growth without any treatment. The *x* axis represents the log of the concentration of each tested compound. [a]For cholinium chloride, the curve was omitted since most tested concentrations displayed no inhibition of activity and the IC_{50} value is an approximate prediction based on the obtained data.

Fig. 5 Dose–response curve and calculated IC_{50} values (in μM, upper right corner) of amphotericin B (AmB, black squares), cetylpyridinium chloride ($[C_{16}py]Cl$, orange hexagons), cetylpyridinium amphotericin B ($[C_{16}py][AmB]$, purple circles) and a equimolar mixture of $[C_{16}py]Cl$ and AmB ($[C_{16}py]Cl + AmB$, pink triangles), against *Aspergillus fumigatus*. The *y* axis represents the percentage of metabolic activity (determined by standard MTT assay) comparatively to the growth without any treatment. The *x* axis represents the log of the concentration of each tested compound.

Interactions with fungal ergosterol

The main proposed models for AmB mechanism of action, from the formation of ion channel aggregates[10] to the sterol sponge model,[11] have in common the interaction of AmB with the main fungal membrane sterol, *i.e.* ergosterol. We performed molecular dynamics simulations to verify if there were any differences between the interaction of ergosterol with AmB or $[C_{16}py][AmB]$. Two types of model system were considered: (i) aqueous solutions containing ergosterol and AmB and (ii) aqueous solutions containing ergosterol and the ionic liquid formulation. Fig. 6 shows relevant aggregate distribution functions along with snapshots of the equilibrated simulation boxes corresponding to the clustering of ergosterol molecules and AmB (Fig. 6A) and ergosterol molecules and $[C_{16}py][AmB]$ (Fig. 6B). The "ergo–AmB" distribution function (Fig. 6A) shows that only 4% of the AmB or ergosterol molecules are not in contact with the other species, and that most of them are part of a very large cluster with maximum probability (96%) around $n_a = 30$ (the maximum possible aggregate size). On the other hand, the "ergo–$[AmB]^-$"

distribution function of the ergosterol–$[C_{16}py][AmB]$ system (Fig. 6B) shows that only 2% of the $[AmB]^-$ anion or ergosterol molecules are not in contact with the other species and that most of them are part of very large clusters with $26 < n_a < 30$ (with a maximum probability around $n_a = 30$). A close behavior was observed for the "ergo–$[C_{16}py]^+$" distribution function (Fig. 6B): only 1% of the $[C_{16}py]^+$ cation or ergosterol molecules are not in contact with the other species and most of them are part of very large cluster around $n_a = 29$. These mixed cation–ergosterol clusters are formed due to favorable interactions between the two species, *i.e.* the dispersion forces between their non-polar moieties (the alkyl chain of the cation and the ergosterol molecule).

The difference between the two systems is more noticeable if one compares the "ergo–ergo" distribution functions of each system. In the ergosterol–AmB system (Fig. 6A), the "ergo–ergo" distribution shows only one aggregate comprising all ergosterol molecules. The "ergo–ergo" distribution function of the ergosterol–$[C_{16}py][AmB]$ system (Fig. 6B) shows that the cluster sizes are part of a distribution of small clusters with $1 < n_a < 10$ (with
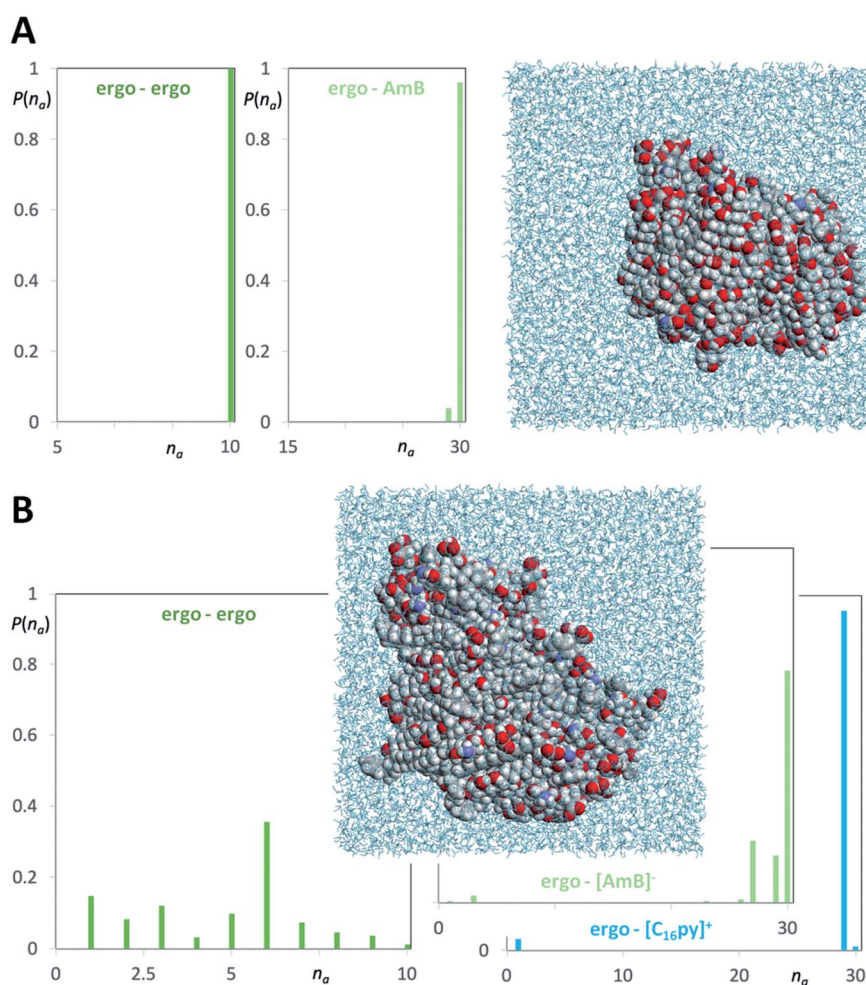
Fig. 6 Molecular dynamics simulation snapshots and discrete probability distribution functions of aggregate sizes ($P(n_a)$) for different aggregate types of ergosterol (ergo), amphotericin B (AmB) and cetylpyridinium amphotericin B ($[C_{16}py][AmB]$). (A) AmB−ergosterol simulations (dark green graph: ergosterol clusters; light green graph: ergosterol−AmB aggregates). (B) $[C_{16}py][AmB]$−ergosterol simulations (deep green graph: ergosterol clusters; light green graph: ergosterol−$[AmB]^-$ anion aggregates; blue graph: ergosterol−$[C_{16}py]^+$ cation aggregates).

Paper

Table 1 Percentage of ergosterol in the supernatant of aqueous mixtures with 20, 30, 40, 50 or 60 μM of AmB, $[C_{16}py][AmB]$ or $[C_{16}py]$ Cl, after precipitation. 20 μM of ergosterol was mixed with of each compound in ultrapure water, incubated for one hour and centrifuged. The supernatant was analyzed by HPLC and the ergosterol content was quantified. The data are presented as the percentage (followed by the standard deviation) of ergosterol present in the supernatant of each mixture relative to ergosterol alone, after precipitation by centrifugation

Concentration (μM)	AmB	$[C_{16}py][AmB]$	$[C_{16}py]Cl$
20	98.70 ± 0.45	70.14 ± 0.35	91.70 ± 2.15
30	85.01 ± 1.78	78.91 ± 2.13	95.94 ± 1.40
40	97.97 ± 3.75	58.68 ± 5.49	92.24 ± 1.31
50	78.52 ± 2.41	72.72 ± 1.26	85.48 ± 0.91
60	99.59 ± 0.30	45.39 ± 1.02	92.67 ± 3.00

a maximum probability around $n_a = 6$). This is due to the fact that the ergosterol is also involved in strong interactions with the $[C_{16}py]^+$ cation. Collectively, the molecular dynamics simulations show that ergosterol interacts more with $[C_{16}py][AmB]$ than with pure AmB. This occurs because ergosterol molecules seem to be embedded in the midst of $[C_{16}py][AmB]$ molecules. While the interaction between sterol and the [AmB] anion exists, the interaction between ergosterol and cation are even stronger, which would justify increased antifungal activity of $[C_{16}py][AmB]$, when compared to pure AmB.

To further support these observations, 20 μM ergosterol was mixed in water with different concentrations of either AmB, $[C_{16}py][AmB]$ or $[C_{16}py]Cl$. The mixtures were incubated for one hour to allow interaction of ergosterol with each compound, and then centrifuged at high speed to allow precipitation. It was expected that higher amounts of ergosterol would precipitate along with the compound that it has greater interaction with. The results depicted in Table 1 show that for all tested concentrations of $[C_{16}py][AmB]$ there was a greater decrease in ergosterol amounts in the supernatant in comparison with either AmB or $[C_{16}py]Cl$. Nearly 50% of ergosterol seemed to precipitate when combined with 60 μM of $[C_{16}py][AmB]$, while the maximum precipitation observed for AmB was around 20% (50 μM of AmB). This is suggestive that ergosterol interacts more with the ionic liquid formulation than with AmB. Moreover, this does not seem to be solely an effect of the cation, since much higher decreases of ergosterol was observed for all concentrations of $[C_{16}py][AmB]$ compared to $[C_{16}py]Cl$ (Table 1).

Evaluation of cytotoxicity

The interaction with membrane sterols is not only underlying the AmB antifungal activity, but it is also one of the most accepted reasons for its high toxicity. This is mainly due to the high structural similarities between ergosterol and cholesterol, the main sterol of animal cells (Fig. S1†). We have performed a MTT metabolic activity assay with mIMCD-3 cells, to determine and compare the cytotoxicity of $[C_{16}py][AmB]$ to the parental compound, AmB. While we calculated an IC$_{50}$ of 42.61

Table 2 Calculated IC$_{50}$ values (in μM) of amphotericin B (AmB), cetylpyridinium amphotericin B ($[C_{16}py][AmB]$) and cetylpyridinium chloride ($[C_{16}py]Cl$) towards mIMCD-3 cells, determined by standard MTT assays

	IC$_{50}$ (μM)
AmB	42.61
$[C_{16}py][AmB]$	0.06
$[C_{16}py]Cl$	0.01

μM for AmB (Table 2), the ionic liquid formulation displayed a much higher cytotoxicity, with an IC$_{50}$ of 0.06 μM (over 700-times higher than AmB). These results are in accordance with previously reported higher cytotoxicity of a cetylpyridinium ampicillin ionic liquid formulation, which displayed IC$_{50}$ values of *ca.* 0.03 and 0.01 μM against skin and gingival fibroblasts, respectively, while for the parental compound (*i.e.* sodium ampicillin) the IC$_{50}$ was above 100 μM.[53] Furthermore, in agreement with previous studies that reported the high cytotoxicity of $[C_{16}py]Cl$, we have registered an IC$_{50}$ of 0.01 μM for this compound (Table 2).

Interactions with cholesterol

Altogether, the data suggest that, as seen for ergosterol, increased interactions between $[C_{16}py][AmB]$ and cholesterol could also be occurring and that the cytotoxicity of the ionic liquid formulation could be greatly influenced by the $[C_{16}py]^+$ cation. Molecular dynamics simulations combining cholesterol with AmB or $[C_{16}py][AmB]$ were performed to identify the interactions between these molecules. Fig. S2† shows relevant aggregate distribution functions along with snapshots of the equilibrated simulation boxes corresponding to the clustering of cholesterol molecules and AmB (Fig. S2A†) and cholesterol molecules and $[C_{16}py][AmB]$ (Fig. S2B†). The "chol–AmB" distribution function in Fig. S2A† shows that the molecules are forming a large cluster with maximum probability (99.9%) around $n_a = 30$ (the maximum size possible for the aggregate in the box), with a small fraction (0.1%) of AmB and cholesterol molecules not in close contact with each other. The "chol–$[AmB]^-$" distribution probability of the cholesterol–$[C_{16}py]$ [AmB] system (Fig. S2B†) shows that there is a large distribution of aggregate sizes, with $1 < n_a < 28$ (maximum probability around $n_a = 19$). For the "chol–$[C_{16}py]^+$" aggregate distribution function, on the other hand, only 0.5% of the $[C_{16}py]^+$ cation or cholesterol molecules are isolated and most of the species are forming a very large cluster around $n_a = 30$ (Fig. S2B†). As seen in the ergosterol–$[C_{16}py][AmB]$ simulations, the dispersion interaction between the alkyl chain of $[C_{16}py]^+$ cation and cholesterol molecule is the main drive of the formation of mixed "chol–$[C_{16}py]^+$" clusters.

Comparison of "chol–chol" distribution functions shows only one large aggregate comprising all cholesterol molecules present in the system with neutral AmB (Fig. S2A†), while the "chol–chol" cluster sizes are distributed between $1 < n_a < 8$ (with a maximum probability around $n_a = 6$) in the presence of

[C_{16}py][AmB] (Fig. S2B†). As seen for "ergo–ergo" distribution functions (Fig. 6A and B), the reduction in "chol–chol" cluster sizes is the result of the strong interactions of the sterol molecules with the [C_{16}py]$^+$ cation (Fig. S2A and B†). Comparing the ergosterol and cholesterol simulations, it is observed that cholesterol exhibits an even bigger interaction with the [C_{16}py]$^+$ cation than ergosterol. The small differences between the structures of ergosterol and cholesterol (Fig. S1†) have been suggested to have little influence in their interaction with AmB.[54] However, it is possible that these differences could in fact influence sterol–[C_{16}py]$^+$ interactions, yet to be disclosed, in ways that would explain a greater affinity of cholesterol towards the cation, compared with ergosterol. This could explain why the IC$_{50}$ values of [C_{16}py][AmB] towards animals cells are lower than those determined for the fungal strains (Fig. 2, 4 and Table 2). It is apparent that interaction with ergosterol or cholesterol occurs mainly between the aliphatic moieties of the cation. Deeper studies need be conducted, aiming at identifying specific modifications in the cation, e.g. double bonds, which could alter its affinity to specific regions in each sterol.

Evaluation of antibacterial activity

One of the most attractive aspects of designing active pharmaceutical ingredients as ionic liquids is the ability to combine the distinct proprieties that come individually from the cation and the anion. This dual nature of ionic liquids has been already explored in the development of active formulations displaying two biological functions (e.g. antimicrobial proprieties and artificial sweeteners).[22] The antibacterial activity of some ionic liquids have been reported to be strongly influenced by the cation, as seen in formulations containing long-chain imidazolium,[55] quinolinium,[56] pyridinium[57] and tetraalkylammonium[42,58] or tetraalkylphosphonium cations.[47] In its chloride form, the [C_{16}py]$^+$ cation has already been explored in human healthcare products, mainly due to its antibacterial properties.[43] It has been used in mouthwash formulations in the United States since the 1940s and, more recently; it has been investigated as a potential antiseptic in other medical applications, e.g. in the treatment and management of chronic wounds.[59]

In our study, we wanted to evaluate whether our formulation with higher antifungal activity, [C_{16}py]AmB, could also display antibacterial properties, as a contribution from the [C_{16}py]$^+$ cation. We selected S. aureus and E. coli as Gram-positive and Gram-negative bacteria models, respectively. As expected, AmB did not inhibit the growth of either bacterium at the maximum concentration tested (predicted IC$_{50}$ values above 100 μM), while [C_{16}py]Cl, displayed antibacterial activity against both E. coli and S. aureus, with calculated IC$_{50}$ values of 13.2 and 3.7 μM, respectively (Table 3). The [C_{16}py][AmB] formulation displayed similar (even slightly stronger) antibacterial activity as [C_{16}py]Cl, with IC$_{50}$ values of 10 μM for the Gram-negative bacterium E. coli and 2.7 μM for the Gram-positive S. aureus (Table 3). Our data show that the combination of [C_{16}py]$^+$ and [AmB]$^-$ results in a formulation with dual biological functionality: the increased antifungal activity, comparatively to pure AmB, combined with the preserved antibacterial properties of the [C_{16}py]$^+$ cation.

Table 3 Calculated IC$_{50}$ values (in μM) of amphotericin B (AmB), cetylpyridinium amphotericin B ([C_{16}py][AmB]) and cetylpyridinium chloride ([C_{16}py]Cl) towards the bacteria Staphylococcus aureus or Escherichia coli, determined by absorbance measurement (OD$_{600}$)

	IC$_{50}$	
	S. aureus	E. coli
AmB	>100	>100
[C_{16}py][AmB]	2.8	10.0
[C_{16}py]Cl	3.7	13.2

Despite its high cytotoxicity, the use of [C_{16}py]Cl in oral hygiene products in concentrations up to 0.1 mg mL^{-1} is approved by the U.S. Food and Drug Administration (https://www.fda.gov). Therefore, pharmacological data is already available to guide the appropriate studies and predict the recommended doses and therapeutics to explore formulations containing the [C_{16}py]$^+$ cation, including the dual activity of [C_{16}py][AmB] against mixed communities of bacteria and fungi.

Conclusions

Creating new opportunities in antifungal therapy is crucial for improving the efficacy of medications already in clinical use, defeating induced resistance and the emergence of novel pathogens. In this study, we evaluated the biological activity of three novel ionic liquid formulations that resulted from the combination of an anionic form of the antifungal drug AmB with three distinct cations: [chol]$^+$, [C_{16}py]$^+$ or [$P_{6,6,6,14}$]$^+$. [$P_{6,6,6,14}$][AmB] led to a decreased antifungal activity and what seems to be a mode of action distinct from the parental antifungal drug. The ionic liquid formulations [chol][AmB] and [C_{16}py][AmB], however, increased AmB antifungal activity 1.2- and 3.2-fold, respectively, either for A. fumigatus or the intrinsically resistant A. terreus. Gene expression analysis seems to indicate that either ionic liquid maintained the mechanism of action of AmB. Deeper investigations on the effects of [C_{16}py][AmB], revealed that an ionic liquid formulation is required for increased antifungal activity, which was not observed with an equimolar combination of the parental compounds, AmB and [C_{16}py]Cl. Molecular dynamics simulations further reveal that the reason behind the increased antifungal activity of [C_{16}py][AmB] is the greater interaction of ergosterol, the main fungal membrane sterol, with the ionic liquid formulation, when compared to AmB (also seen experimentally). The simulations show that the augmented antifungal activity is influenced by the close interactions observed between ergosterol and the [C_{16}py]$^+$ cation when combined with the anionic AmB. Even greater seems to be the interaction of cholesterol, the main animal sterol, with [C_{16}py]$^+$, which seems to justify the high cytotoxicity of [C_{16}py][AmB], as well as of the parental compound [C_{16}py]Cl.

These data set ground to further exploring ionic liquid formulations as alternative solutions for enhanced administrations and antifungal activity of AmB, as well as other antifungal drugs. It emphasizes that molecular studies are crucial

for the deep understanding of the interactions between ionic liquid formulations and the biological targets of AmB, *i.e.* membrane sterols. Our results can be used as a guide towards the fine-tuning and development of AmB-based ionic liquid formulations that selectively target ergosterol in detriment of cholesterol, resulting in effective antifungal agents with low cytotoxicity.

Furthermore, [C₁₆py][AmB] not only presented increased antifungal activity, but was also effective against the bacteria *S. aureus* and *E. coli*, indicating a preservation of the antibacterial properties of the parental compound [C₁₆py]Cl. This ionic liquid formulation is based on two pharmaceutical ingredients approved by the regulating authorities, which can guide and facilitate the necessary studies for its use. One conceived strategy for the application of this new dual functional formulation in the near future is to consider their slow release from patches for wound care of chronic wounds which frequently contain a mixed microbiota of bacteria and fungi.

Conflicts of interest

There are no conflicts to declare.

Acknowledgements

References

1 G. D. Brown, D. W. Denning, N. A. R. Gow, S. M. Levitz, M. G. Netea and T. C. White, *Sci. Transl. Med.*, 2012, **4**, 165rv113.

2 K. J. Kwon-Chung and J. A. Sugui, *PLoS Pathog.*, 2013, **9**, e1003743.

3 A. Beauvais, C. Schmidt, S. Guadagnini, P. Roux, E. Perret, C. Henry, S. Paris, A. Mallet, M. C. Prévost and J. P. Latgé, *Cell. Microbiol.*, 2007, **9**, 1588–1600.

4 E. Mowat, J. Butcher, S. Lang, C. Williams and G. Ramage, *J. Med. Microbiol.*, 2007, **56**, 1205–1212.

5 M. K. Kathiravan, A. B. Salake, A. S. Chothe, P. B. Dudhe, R. P. Watode, M. S. Mukta and S. Gadhwe, *Bioorg. Med. Chem.*, 2012, **20**, 5678–5698.

6 P. E. Verweij, E. Snelders, G. H. Kema, E. Mellado and W. J. Melchers, *Lancet Infect. Dis.*, 2009, **9**, 789–795.

7 C. Jiménez-Ortigosa, C. Moore, D. W. Denning and D. S. Perlin, *Antimicrob. Agents Chemother.*, 2017, **61**, e01277–17.

8 M.-Y. S. Moosa, G. J. Alangaden, E. Manavathu and P. H. Chandrasekar, *J. Antimicrob. Chemother.*, 2002, **49**, 209–213.

9 R. J. Hamill, *Drugs*, 2013, **73**, 919–934.

10 D. M. Kamiński, *Eur. Biophys. J.*, 2014, **43**, 453–467.

11 T. M. Anderson, M. C. Clay, A. G. Cioffi, K. A. Diaz, G. S. Hisao, M. D. Tuttle, A. J. Nieuwkoop, G. Comellas, N. Maryum, S. Wang, B. E. Uno, E. L. Wildeman, T. Gonen, C. M. Rienstra and M. D. Burke, *Nat. Chem. Biol.*, 2014, **10**, 400–406.

12 P. Gautam, J. Shankar, T. Madan, R. Sirdeshmukh, C. S. Sundaram, W. N. Gade, S. F. Basir and P. U. Sarma, *Antimicrob. Agents Chemother.*, 2008, **52**, 4220–4227.

13 G. Blum, S. Perkhofer, H. Haas, M. Schrettl, R. Würzner, M. P. Dierich and C. Lass-Flörl, *Antimicrob. Agents Chemother.*, 2008, **52**, 1553–1555.

14 J. P. Botero Aguirre and A. M. Restrepo Hamid, *Cochrane Database Syst. Rev.*, 2015, CD010481, DOI: 10.1002/ 14651858.CD010481.pub2.

15 R. Herbrecht, S. Natarajan-Amé, Y. Nivoix and V. Letscher-Bru, *Expert Opin. Pharmacother.*, 2003, **4**, 1277–1287.

16 J. M. Michot, C. Gubavu, E. Fourn, G. Maigne, E. Teicher, A. Angoulvant, S. Blanche, O. Lortholary, A. Coilly, J. C. Duclos-Vallée, M. Sebagh, C. Guettier, C. Aumont, J. F. Delfraissy and O. Lambotte, *Int. J. Antimicrob. Agents*, 2014, **43**, 566–569.

17 H. Van de Ven, C. Paulussen, P. B. Feijens, A. Matheeussen, P. Rombaut, P. Kayaert, G. Van den Mooter, W. Weyenberg, P. Cos, L. Maes and A. Ludwig, *J. Controlled Release*, 2012, **161**, 795–803.

18 P. D. McCrary, P. A. Beasley, G. Gurau, A. Narita, P. S. Barber, O. A. Cojocaru and R. D. Rogers, *New J. Chem.*, 2013, **37**, 2196–2202.

19 N. V. Plechkova and K. R. Seddon, *Chem. Soc. Rev.*, 2008, **37**, 123–150.

20 M. Petkovic and C. Silva Pereira, in *Ionic Liquids UnCOILed: Critical Expert Overviews*, ed. N. V. Plechkova and K. R. Seddon, John Wiley & Sons, Inc., New Jersey, 2012, pp. 283–303, DOI: 10.1002/9781118434987.ch9.

21 A. Balk, U. Holzgrabe and L. Meinel, *Eur. J. Pharm. Biopharm.*, 2015, **94**, 291–304.

22 W. L. Hough-Troutman, M. Smiglak, S. Griffin, W. M. Reichert, I. Mirska, J. Jodynis-Liebert, T. Adamska, J. Nawrot, M. Stasiewicz, R. D. Rogers and J. Pernak, *New J. Chem.*, 2009, **33**, 26–33.

23 C. Suresh, H. Zhao, A. Gumbs, C. S. Chetty and H. S. Bose, *Bioorg. Med. Chem. Lett.*, 2012, **22**, 1734–1738.

24 J. M. M. Araújo, C. Florindo, A. B. Pereiro, N. S. M. Vieira, A. A. Matias, C. M. M. Duarte, L. P. N. Rebelo and I. M. Marrucho, *RSC Adv.*, 2014, **4**, 28126–28132.

25 R. Ferraz, V. Teixeira, D. Rodrigues, R. Fernandes, C. Prudêncio, J. P. Noronha, Ž. Petrovski and L. C. Branco, *RSC Adv.*, 2014, **4**, 4301–4307.

26 R. Ferraz, D. Silva, A. R. Dias, V. Dias, M. M. Santos, L. Pinheiro, C. Prudêncio, J. P. Noronha, Ž. Petrovski and L. C. Branco, *Pharmaceutics*, 2020, **12**, 221.

27 O. A. Cojocaru, J. L. Shamshina, G. Gurau, A. Syguda, T. Praczyk, J. Pernak and R. D. Rogers, *Green Chem.*, 2013, **15**, 2110–2120.

28 J. Pernak, B. Markiewicz, A. Zgoła-Grześkowiak, Ł. Chrzanowski, R. Gwiazdowski, K. Marcinkowska and T. Praczyk, *RSC Adv.*, 2014, **4**, 39751–39754.

29 M. Cokol-Cakmak and M. Cokol, *Methods Mol. Biol.*, 2019, **1939**, 3–9.

30 J. N. Canongia Lopes and A. A. H. Pádua, *J. Phys. Chem. B*, 2004, **108**, 16893–16898.

31 W. L. Jorgensen, D. S. Maxwell and J. Tirado-Rives, *J. Am. Chem. Soc.*, 1996, **118**, 11225–11236.

32 M. Praprotnik, D. Janežič and J. Mavri, *J. Phys. Chem. A*, 2004, **108**, 11056–11062.

33 W. Smith and T. R. Forester, *The DL_POLY package of molecular simulation routines, version 2.2*, The Council for The Central Laboratory of Research Councils, Daresbury Laboratory, Warrington, UK, 2006.

34 H. Bekker, H. Berendsen, E. J. Dijkstra, S. Achterop, R. Drunen, D. van der Spoel, A. Sijbers, H. Keegstra, B. Reitsma and M. K. R. Renardus, *Presented in part at the Physics Computing '92*, Prague, 1993.

35 H. J. C. Berendsen, D. van der Spoel and R. van Drunen, *Comput. Phys. Commun.*, 1995, **91**, 43–56.

36 D. Van Der Spoel, E. Lindahl, B. Hess, G. Groenhof, A. E. Mark and H. J. C. Berendsen, *J. Comput. Chem.*, 2005, **26**, 1701–1718.

37 S. Páll, M. J. Abraham, C. Kutzner, B. Hess and E. Lindahl, *Presented in part at the International Conference on Exascale Applications and Software 2014*, Cham, 2015.

38 M. J. Abraham, T. Murtola, R. Schulz, S. Páll, J. C. Smith, B. Hess and E. Lindahl, *SoftwareX*, 2015, **1–2**, 19–25.

39 L. Martinez, R. Andrade, E. G. Birgin and J. M. Martinez, *J. Comput. Chem.*, 2009, **30**, 2157–2164.

40 C. E. S. Bernardes, K. Shimizu, A. I. M. C. Lobo Ferreira, L. M. N. B. F. Santos and J. N. Canongia Lopes, *J. Phys. Chem. B*, 2014, **118**, 6885–6895.

41 P. Markham, G. D. Robson, B. W. Bainbridge and A. P. J. Trinci, *FEMS Microbiol. Rev.*, 1993, **104**, 287–300.

42 M. Petkovic, J. L. Ferguson, H. Q. N. Gunaratne, R. Ferreira, M. C. Leitão, K. R. Seddon, L. P. N. Rebelo and C. Silva Pereira, *Green Chem.*, 2010, **12**, 643–649.

43 C. D. Wu and E. D. Savitt, *Periodontol. 2000*, 2002, **28**, 91–105.

44 K. Bica, C. Rijksen, M. Nieuwenhuyzen and R. D. Rogers, *Phys. Chem. Chem. Phys.*, 2010, **12**, 2011–2017.

45 R. F. M. Frade, A. A. Rosatella, C. S. Marques, L. C. Branco, P. S. Kulkarni, N. M. M. Mateus, C. A. M. Afonso and C. M. M. Duarte, *Green Chem.*, 2009, **11**, 1660–1665.

46 Y. Zhao, P. Paderu, S. Park, A. Dukhan, M. Senter and D. S. Perlin, *Antimicrob. Agents Chemother.*, 2012, **56**, 2770.

47 M. Petkovic, D. O. Hartmann, G. Adamová, K. R. Seddon, L. P. N. Rebelo and C. Silva Pereira, *New J. Chem.*, 2012, **36**, 56–63.

48 D. O. Hartmann and C. Silva Pereira, *New J. Chem.*, 2013, **37**, 1569–1577.

49 C. M. S. S. Neves, P. J. Carvalho, M. G. Freire and J. A. P. Coutinho, *J. Chem. Thermodyn.*, 2011, **43**, 948–957.

50 G. Blum, B. Kainzner, K. Grif, H. Dietrich, B. Zeiger, T. Sonnweber and C. Lass-Flörl, *Clin. Microbiol. Infect.*, 2013, **19**, 50–55.

51 B. Kirchner, F. Malberg, D. S. Firaha and O. Hollóczki, *J. Phys.: Condens. Matter*, 2015, **27**, 463002.

52 R. Matsumoto, M. W. Thompson and P. T. Cummings, *J. Phys. Chem. B*, 2019, **123**, 9944–9955.

53 R. Ferraz, J. Costa-Rodrigues, M. H. Fernandes, M. M. Santos, I. M. Marrucho, L. P. Rebelo, C. Prudêncio, J. P. Noronha, Ž. Petrovski and L. C. Branco, *ChemMedChem*, 2015, **10**, 1480–1483.

54 M. Baran, E. Borowski and J. Mazerski, *Biophys. Chem.*, 2009, **141**, 162–168.

55 L. Carson, P. K. W. Chau, M. J. Earle, M. A. Gilea, B. F. Gilmore, S. P. Gorman, M. T. McCann and K. R. Seddon, *Green Chem.*, 2009, **11**, 492–497.

56 A. Busetti, D. E. Crawford, M. J. Earle, M. A. Gilea, B. F. Gilmore, S. P. Gorman, G. Laverty, A. F. Lowry, M. McLaughlin and K. R. Seddon, *Green Chem.*, 2010, **12**, 420–425.

57 J. Pernak, J. Kalewska, H. Ksycińska and J. Cybulski, *Eur. J. Med. Chem.*, 2001, **36**, 899–907.

58 J. Pernak, M. Smiglak, S. T. Griffin, W. L. Hough, T. B. Wilson, A. Pernak, J. Zabielska-Matejuk, A. Fojutowski, K. Kita and R. D. Rogers, *Green Chem.*, 2006, **8**, 798–806.

59 C. Fromm-Dornieden, J.-D. Rembe, N. Schäfer, J. Böhm and E. K. Stuermer, *J. Med. Microbiol.*, 2015, **64**, 407–414.